Combined Brownian Dynamics and Spectral Simulation of the Recovery of Polymeric Fluids after Shear Flow

T. W. Bell, G. H. Nyland, J. J. de Pablo, and M. D. Graham*

Department of Chemical Engineering and Rheology Research Center, University of Wisconsin−Madison, Madison, Wisconsin 53706-1691

Received February 21, 1996; Revised Manuscript Received January 15, 1997[⊗]

ABSTRACT: The constrained recovery of polymeric fluids following cessation of steady shear flow is studied using linear bead−spring chain models for dilute polymer solutions and the Curtiss−Bird model for polymer melts. Brownian dynamics simulation techniques are combined with a spectral method for solution of the continuum equation of motion. The shear stress required to solve the continuum equation is computed directly from ensemble averages over internal configurations of model molecules, thereby eliminating the need for a closed-form constitutive equation. Simultaneous solution of the equation of motion for actual fluid velocities obviates the linear velocity profile assumption used in previous studies of constrained recoil. For each of the models examined in the present work, a maximum was observed in the overall recovery with increasing steady-state shear rate. These maxima are an inherent consequence of the polymer models' shear thinning behavior but are more pronounced if the assumption of a linear velocity profile is relaxed.

1. Introduction

In the presence of a strong flow field, the backbones of long polymer chains in solution or in a melt tend to align with the direction of the flow. When the driving force for the flow is removed, molecules are left in nonequilibrium configurations. If the longest relaxation time for the polymer is of the same order or greater than the characteristic time of the flow, *i.e.* when the Deborah number De ∼ $O(1)$, the relaxation of polymer molecules back to equilibrium can be macroscopically observed as flow to some previously occupied position. Such behavior is termed recovery or recoil.[1]

Molecular models of polymers provide substantial insight about the rheological behavior of real polymeric fluids. Unfortunately, their use is often hampered by the complexity or even nonexistence of a closed form constitutive equation. Only recently have molecular models been used to study recovery flows, which occur in extrusion and other industrially important processes. Borgbjerg *et al.*[2] have presented a Brownian dynamics study of recovery following simple steady shear flow in a parallel-plate geometry using the polymer melt kinetic theory of Curtiss and Bird.[3] These authors showed that the recovery predicted by the Curtiss−Bird model exhibits a maximum at high shear rates. However, the transient shear rate was calculated in their simulations through the zero shear stress boundary condition on the moving plate assuming a linear velocity profile in the fluid. While this approximation is justified for small separations between the two plates, the actual velocity profiles for larger gaps may be far from linear and may have important effects on the overall recovery of the fluid.

The present work extends this study by combining Brownian dynamics and spectral techniques to simultaneously obtain the polymer contribution to the shear stress and solve the macroscopic momentum equation for the velocity profile. This approach follows from the work of Öttinger and Laso,[4] who combine stochastic simulation techniques with finite elements in macroscopic flow calculations. A spectral discretization of the momentum equation replaces finite elements in the present work due to the attractive convergence properties of spectral techniques. Both Brownian dynamics and continuum calculations are executed at every time step of a flow simulation. The Brownian dynamics calculations provide the required shear stresses in the fluid. These stresses are then used to simultaneously solve the macroscopic momentum equation for the velocity profile, thereby eliminating the need for a closed-form constitutive equation. While this approach allows the linear velocity profile assumption to be removed, Brownian dynamics simulations require significant amounts of computer time. The use of spectral techniques in place of finite elements is largely motivated by a need to increase the efficiency of macroscopic flow calculations.

2. Brownian Dynamics

Two types of polymeric fluid models are investigated in the present work: the freely jointed linear bead−spring model for dilute polymer solutions and the Curtiss−Bird model for polymer melts.

The dynamic behavior of bead−spring chains is described in polymer kinetic theory by a diffusion equation for the probability density function ψ of the internal configurations of the model. If $\mathbf{r}_j$ is used to denote the coordinates of bead j, then the diffusion equation for the bond vectors $\mathbf{Q}_j = \mathbf{r}_{j+1} - \mathbf{r}_j$ of a bead−spring chain with N beads can be written[3,5]

$$\frac{\partial \psi}{\partial t} = -\sum_j \frac{\partial}{\partial \mathbf{Q}_j}\left\{[\kappa\cdot\mathbf{Q}_j]\psi - \frac{1}{\zeta}\sum_k A_{jk}\left(kT\frac{\partial}{\partial \mathbf{Q}_k} + \mathbf{F}_k^c\right)\psi\right\} \quad (1)$$

where the transpose of the velocity gradient tensor is denoted by κ, kT is the product of Boltzmann's constant and the temperature, ζ is the hydrodynamic friction coefficient of a spherical bead, and A_{jk} are the elements of the Rouse matrix. The connector force associated with spring k is denoted by $\mathbf{F}_k^c$. Brownian dynamics simulations take advantage of the equivalence between the partial differential diffusion eq 1 and a system of stochastic differential equations (SDEs).[6,7] In the case of bead−spring chains, the equivalent SDE system can be written as[5]

[⊗] Abstract published in *Advance ACS Abstracts,* March 1, 1997.

S0024-9297(96)00268-9 CCC: $14.00 © 1997 American Chemical Society

$$d\mathbf{Q}_j = \left\{[\kappa\cdot\mathbf{Q}_j] - \frac{1}{\zeta}\sum_k A_{jk}\mathbf{F}_k^c\right\} dt + \sqrt{\frac{2kT}{\zeta}}[d\mathbf{W}_{j+1} - d\mathbf{W}_j] \quad (2)$$

where $\mathbf{W}_j$ is the Wiener process, discussed below. In this work, the bead connectors are taken to be *F*initely *E*xtensible *N*onlinear *E*lastic or FENE springs, which approximate the inverse Langevin spring force law by[8]

$$\mathbf{F}_k^c = \frac{H\mathbf{Q}_k}{1 - Q_k^2/(bkT/H)} \quad (3)$$

where H is the spring force constant. The dimensionless parameter describing the finite extensibility of the spring is given by $b = HQ_o^2/kT$, where Q_o is the maximum allowable extension. If the normal modes $\mathbf{Q}'_j$ of the FENE chain are introduced by diagonalizing the Rouse matrix and the rotated bond vectors are nondimensionalized by $\mathbf{Q}'^*_j = \sqrt{H/kT}Q'_j$, the Euler time discrete approximation to eq 2 at time $t_n = n\Delta t$ can be shown to be

$$\mathbf{Q}'^{*(n+1)}_k = \mathbf{Q}'^{*(n)}_k + [\kappa\cdot\mathbf{Q}'^{*(n)}_k]\Delta t - \frac{a_k}{4\lambda_H}\frac{\mathbf{Q}'^{*(n)}_k}{1 - Q'^{*(n)2}_k/b}\Delta t + \sqrt{\frac{a_k}{2\lambda_H}\Delta t}\mathbf{W}_k^{(n)} \quad (4)$$

where $\lambda_H = \zeta/4H$ is the characteristic relaxation time of the springs and $a_k = 4\sin^2(k\pi/2N)$ are the eigenvalues of the Rouse matrix. The components of the vectors $\mathbf{W}_k^{(n)}$ are independent Gaussian random numbers with mean zero and unit variance and are uncorrelated in successive time steps. The three terms of eq 4 correspond to the deformation and orientation of the chain segment due to fluid flow, the contracting force exerted by the spring, and the fluctuating (Brownian) force due to collisions occurring continuously between the beads of the chain and surrounding solvent molecules, respectively. When a large ensemble of chains is simulated according to eq 4, the polymer contribution to the stress tensor can be computed using the Kramers form of the stress tensor[3] according to

$$\boldsymbol{\tau}^p = (N-1)nkT\boldsymbol{\delta} - nkT\sum_k\left\langle\frac{\mathbf{Q}'^*_k\mathbf{Q}'^*_k}{1 - Q'^{*2}_k/b}\right\rangle \quad (5)$$

where n is the polymer number density and where the brackets denote an ensemble average.

The Curtiss−Bird (CB) model[3] for polymer melts is based on the kinetic theory of Kramers freely jointed bead−rod chains. In the Curtiss−Bird model, the constrained environment that polymer molecules experience in a melt or a concentrated solution is described by assuming that hydrodynamic friction forces are anisotropic. The many chain problem is reduced to that of a single reptating chain immersed in an effective mean-field continuum. The diffusion equation for the Curtiss−Bird model is given by

$$\frac{\partial f}{\partial t} = \frac{1}{\lambda}\frac{\partial^2 f}{\partial s^2} - \frac{\partial}{\partial\mathbf{u}}\cdot(\kappa\cdot\mathbf{u} - \kappa:\mathbf{uuu})f \quad (6)$$

where $f(\mathbf{u},s,t)$ is the distribution function governing the probability that a chain segment has an orientation $\mathbf{u}$ at a position along the chain backbone $s \in [0,1]$. The parameter λ, sometimes called the disengagement or reptation time, is the characteristic time constant for the melt. Since the ends of a chain are assumed to be oriented at random, the boundary conditions for the distribution function are $f(\mathbf{u},0,t) = f(\mathbf{u},1,t) = 1/4\pi$. The stochastic differential equations equivalent to eq 6 are

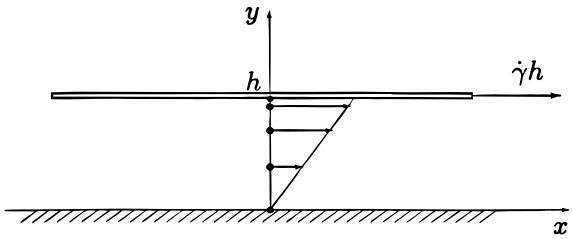

Figure 1. Geometry for parallel plate shear flows in a gap of width h. The linear velocity profile attained during steady-state shear flow is shown prior to the start of the recovery simulation. The positions associated with Chebyshev−Gauss−Lobatto nodes are depicted for nine collocation points.

$$d\mathbf{u} = (\kappa\cdot\mathbf{u} - \kappa:\mathbf{uuu})\,dt \quad (7)$$

$$ds = \sqrt{\frac{2}{\lambda}}\,dW$$

Or, applying the Euler discrete approximation at time $t_n = n\Delta t$

$$\mathbf{u}^{(n+1)} = \frac{\mathbf{u}^{(n)} + (\kappa\cdot\mathbf{u}^{(n)})\Delta t}{|\mathbf{u}^{(n)} + (\kappa\cdot\mathbf{u}^{(n)})\Delta t|} \quad (8)$$

$$s^{(n+1)} = s^{(n)} + \sqrt{\frac{2\Delta t}{\lambda}}W^{(n)}$$

The norm in the denominator of the first discrete equation ensures that the deterministic vector $\mathbf{u}$ is normalized to unity after every time step. Reflections of the stochastic variable s at the boundaries are detected and treated according to procedures described in the literature.[5] For the geometry studied in the present paper, the yx component of the polymer stress tensor is given by

$$\tau^p_{yx} = NnkT\{-\langle u_x u_y\rangle - \lambda\epsilon\dot\gamma\langle s(1-s)u_x^2 u_y^2\rangle\} \quad (9)$$

where $\dot\gamma$ is the time-dependent shear rate and the link-tension coefficient ϵ is a parameter that governs the anisotropy of the hydrodynamic friction tensor.

3. Spectral Solution of the Continuum Equation

Simple shear flows are constructed by containing an incompressible fluid between two parallel plates of infinite length separated by a distance h. If the x-coordinate is taken to be the direction in which one of the plates will move, the velocity in the y and z directions are identically zero at all times (see Figure 1). The velocity in the x-direction is assumed to be of the form $u = u(y,t)$, and the equation of continuity is satisfied trivially. The only relevant equation of motion for polymer fluids is then

$$\rho\frac{\partial u}{\partial t} = \eta_s\frac{\partial^2 u}{\partial y^2} - \frac{\partial}{\partial y}\tau^p_{yx} \quad (10)$$

where ρ is the fluid density, η_s is the viscosity of the

solvent ($\eta_s = 0$ for the Curtiss−Bird melt calculations), and τ^p_{yx} is the polymer contribution to the shear stress.

In the spectral approach, the continuum eq 10 is solved using Chebyshev collocation as opposed to the finite element method originally proposed by Öttinger.[5] Spectral techniques were chosen since, if $N + 1$ represents the number of collocation points used, the error decays more rapidly than any finite power of $1/N$, as $N \to \infty$.[9] This should be contrasted with typical finite element methods, where the error decays as N^{-1} or N^{-2}.[10] This rapid convergence is the primary motivation for implementing a spectral method in Brownian dynamics simulations; not because spectral methods yield highly accurate solutions when a large number of points are employed but rather that they are very accurate for small N. This is particularly important in Brownian dynamics simulations, since a statistically significant ensemble of stochastic trajectories must be integrated at each collocation point and updated at every time step in order to determine the stress in the fluid.

In spectral methods the approximate solution to the one-dimensional partial differential equation $\partial f/\partial t = M(f)$ (where all the spatial derivatives of f are contained in the operator M) is represented as the truncated Fourier series

$$f^N(y,t) = \sum_{k=0}^{N} a_k(t)\phi_k(y) \tag{11}$$

If the trial functions $\phi_k(y)$ are chosen to be the Chebyshev polynomials $\phi_k(y) = T_k(y) = \cos[k \arccos(y)]$ for $k = 0, 1, ..., N$, a convenient choice for the collocation points are the Chebyshev−Gauss−Lobatto points $y_j = \cos(\pi j/N)$. With this subsitution, the trial functions become simply $\phi_k(y) = T_k(y) = \cos(\pi jk/N)$. It can be shown[11] that in Chebyshev−Gauss−Lobatto collocation the Fourier coefficients of eq 11 are given by

$$a_k(t) = \frac{2}{N\bar{c}_k}\sum_{j=0}^{N}\frac{1}{\bar{c}_j} f^N(y_j,t)\cos\left(\frac{\pi jk}{N}\right) \tag{12}$$

for $k = 0, 1, ..., N$. The constant $\bar{c}_j = 2$ for $j = 0$ or $j = N$, and $\bar{c}_j = 1$ if $j = 1, 2, ..., N - 1$. Differentiation of the truncated Fourier series (11) gives

$$\frac{\partial^m f^N}{\partial y^m} = \sum_{k=0}^{N} a_k^{(m)}(t)\cos\left(\frac{\pi jk}{N}\right) \tag{13}$$

where $a_{N+1}^{(m)}(t) = a_N^{(m)}(t) = 0$, and $a_k^{(m)}$ are found using the recursive relationship

$$a_k^{(m)}(t) = \frac{1}{\bar{c}_k}[a_{k+2}^{(m)}(t) + 2(k+1)a_{k+1}^{(m-1)}(t)] \tag{14}$$

for $k = N - 1, N - 2, ..., 0$.

The simplest time discrete version of eq 10 (an explicit Euler method) can be written as

$$u(t + \Delta t,y) = u(t,y) + \frac{\eta_s}{\rho}\frac{\partial^2 u(t,y)}{\partial y^2}\Delta t - \frac{1}{\rho}\frac{\partial}{\partial y}\tau^p_{yx}(t,y)\Delta t \tag{15}$$

At every time step of the simulation, the functions u and τ^p_{yx} are approximated by Fourier series of the form of eq 11 with coefficients a_k and b_k respectively; a_k and b_k are found from eq 12. The spatial derivatives of these functions required by eq 15 are then computed using eq 13, with coefficients recursively obtained as in (14).

The Chebyshev−Gauss−Lobatto collocation points as defined above take on values in the region between $y = -1$ and $y = 1$. Chebyshev collocation naturally assigns a proportionally larger fraction of the points to the neighborhood of exterior boundaries, where the largest velocity gradients in many flow experiments are expected to occur. The simulations are restricted to the interval $y \in [0,1]$ by imposing the antisymmetry condition $u(y) = -u(-y)$, the symmetry condition $\tau^p_{yx}(y) = \tau^p_{yx}(-y)$, and performing calculations only in the region of interest.

In the spectral method, a Brownian dynamics simulation is carried out for an ensemble of stochastic trajectories at each collocation point. The overall simulation is thus the computation of eq 15 with the evaluation of eq 5 (for bead−spring models) or eq 9 (for the Curtiss−Bird model) to determine τ^p_{yx} at each collocation point. In general, each ensemble of trajectories must be placed on a material point of the flow (i.e. a point moving with the fluid velocity). However, the one-dimensional flow studied here is exceptional since the y-position of each material point does not change; material points always coincide with collocation points. In two- and three-dimensional flows, material points and collocation points do not coincide. Interpolation is required to evaluate the velocity gradients on the material points (where the stochastic simulations are performed) and to evaluate the stresses on the collocation points (where the momentum equation is solved). Both one-dimensional results with evenly spaced material points (which do not coincide with collocation points) and preliminary two-dimensional results in a nontrivial geometry[12] show that spectral convergence of the simulations can be maintained if polynomial interpolation of the same order as the collocation method is used.

In numerical simulations of FENE chains in this work, values of the relevant constants were chosen to be those found in ref 4, namely $h = 1.0$, $\rho = 1.2757$, $\lambda_H = 49.62$, $b = 50.0$, $\eta_s = 0.0521$, and the FENE dumbbell zero shear rate viscosity $\eta_o = 1.0$. To scale the results for different chain lengths, nkT is computed as

$$nkT = \frac{\eta_o - \eta_s}{\lambda_H(N-1)}\frac{b+5}{b} \tag{16}$$

This causes the polymer contribution to the shear stress to be nearly equal for all chain lengths, as shown below. The dimensionless quantities which describe the flow are the Deborah number $De = \lambda_H\dot{\gamma}$, and the Reynolds number $Re = (h^2\rho\dot{\gamma})/\eta_o$. Recovery simulations were performed over a range of steady shear rates corresponding to Deborah numbers $De \in O(0.1, 100)$ and Reynolds numbers $Re \in O(0.01, 1)$.

For Curtiss−Bird simulations, the density ρ and the quantity $NnkT$ were both set to unity. The link-tension coefficient was varied from $\epsilon = 0.1$ to $\epsilon = 0.3$ and a relaxation (reptation) time of $\lambda = 400$ was chosen. Recovery simulations were performed over a range of steady shear rates corresponding to Deborah numbers $De \in O(1,1000)$ and Reynolds numbers $Re \in O(0.001, 0.1)$.

4. Recovery Simulations

The recovery simulations investigated here are carried out in two stages. First, a steady-state flow field

is established by setting the top plate in motion at a constant velocity $u = \dot{\gamma}h$ and performing the simulation until a linear steady-state velocity profile and a constant stress profile are observed. Once steady state is attained, the shear boundary condition at the top plate is replaced by the "constrained recoil" boundary condition $\tau_{yx} = 0$. Since the distance between the plates is fixed, the fluid is constrained to move only in the x-direction. During shear recovery, the velocity profile in the fluid is time dependent. The new velocity at the top plate is calculated directly from the zero-shear-stress boundary condition. For the models examined in this work, a general equation for the strain rate at $y = h$ when $\tau_{yx} = 0$ can be written in the form

$$F - \dot{\gamma}G = 0 \tag{17}$$

The appropriate equations for the polymer contribution to τ_{yx}^{p} are eq 5 for the bead−spring models and eq 9 for the CB model. The expression for the velocity gradient at the top plate (which occurs for $j = 0$ using Chebyshev−Gauss−Lobatto collocation points) is then

$$\dot{\gamma}(y=h,t) = \left.\frac{\partial u}{\partial y}\right|_{y=h,t} = \sum_{k=0}^{N} a_k^{(1)}(t) \tag{18}$$

The top plate velocity is set by finding the value $u(y=h,t)$ which causes $\dot{\gamma}$ computed from the spectral coefficients in eq 18 to take on the value computed from eq 17.

5. Results and Discussion

To quantify the degree of recovery in the fluid after the removal of shear, the experimentally measurable "overall recovery", defined by

$$-\gamma_t = -\lim_{t\to\infty}\frac{1}{h}\int_0^t u(y=h,t')\,dt' \tag{19}$$

was computed. This quantity is a ratio of the distance the top plate recoils with respect to the gap width between the shearing plates. In the limit of linear velocity profiles, the overall recovery reduces to the standard definition of the ultimate recoil[1]

$$-\gamma_\infty = -\lim_{t\to\infty}\int_0^t \dot{\gamma}_{yx}(t')\,dt' \tag{20}$$

The validity of the spectral approach was verified by comparing simulation results of overall recovery for a dilute solution of Hookean dumbbells to those of the continuum-mechanical Oldroyd-B model. A dilute solution of Hookean dumbbells is one of the few models whose kinetic theory can be solved exactly; the resulting constitutive equation corresponds to the Oldroyd-B model. Figure 2 shows that the results of recovery calculations for Hookean dumbbells and the Oldroyd-B model are identical within statistical uncertainty. Figure 2 also displays the overall recovery obtained for FENE dumbbells both by assuming a linear velocity profile in the fluid and by performing the spectral simulations to compute the actual velocity profile. The finitely-extensible dumbbells exhibit a maximum in overall recovery in both cases, whereas the recovery of Hookean dumbbells only shows slight curvature at higher shear rates. Hookean dumbbells are unphysical in that the polymer contribution to the solution viscosity is constant at all shear rates; they do not shear thin. FENE dumbbells exhibit shear thinning behavior, however, and this is the principal mechanism for the

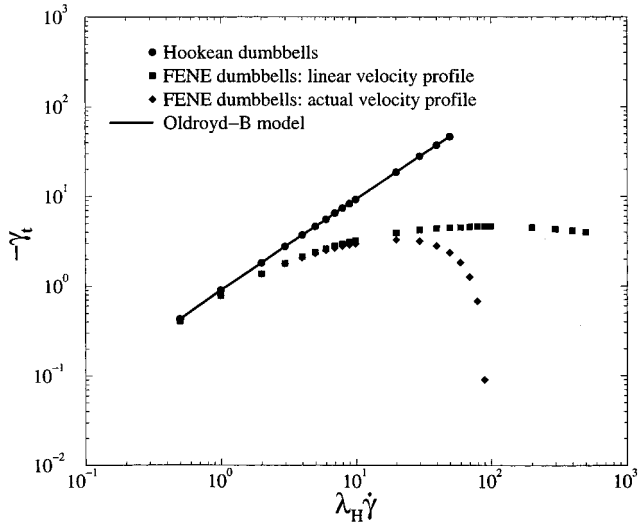

Figure 2. Overall recovery $-\gamma_t$ for dilute solutions of Hookean and FENE dumbbells and the Oldryoyd-B model as a function of the Deborah number $\lambda_H\dot{\gamma}$.

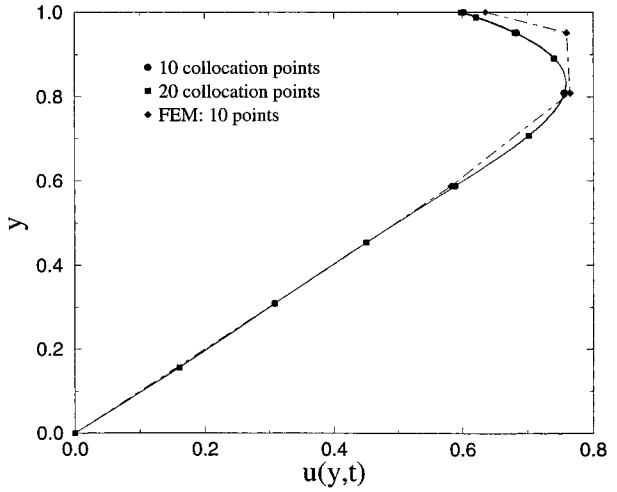

Figure 3. Velocity profile at $t = 0.2$ after the onset of recovery for a dilute solution of FENE dumbbells at De = 49.62 and Re = 1.2757. Curves corresponding to the use of 10 and 20 spectral collocation points are shown, as well as the solution obtained from a 10-point finite element method (FEM).

observed maximum in the recovery curve. For high shear rates the polymer contribution to the shear stress, and therefore to the solution viscosity, becomes small. Inertial effects begin to dominate the diminishing elastic response of the dilute solution, and the recovery decreases. The overall recovery at very high shear rates even becomes negative, an effect that can be accounted for only by inertial considerations. Figure 2 shows that the overall recovery of FENE dumbbells is much more strongly influenced in simulations for which the actual velocities have been computed. This phenomenon is discussed below.

It was found that for calculations performed in the present work, 10 Chebyshev−Gauss−Lobato collocation points were sufficient to spatially discretize the flow. Figure 3 shows the velocity profiles at $t = 0.2$ after the onset of recovery in the full spectral simulation of a dilute solution of FENE dumbbells. Simulations at a shear rate of De $= \lambda_H\dot{\gamma} = 49.62$ (a point near the maximum in Figure 3) for 10 and 20 collocation points yield identical results, indicating that the spectral solution is fully convergent with only 10 nodes. Due to the symmetry of the problem, only 6 of the 10 nodes

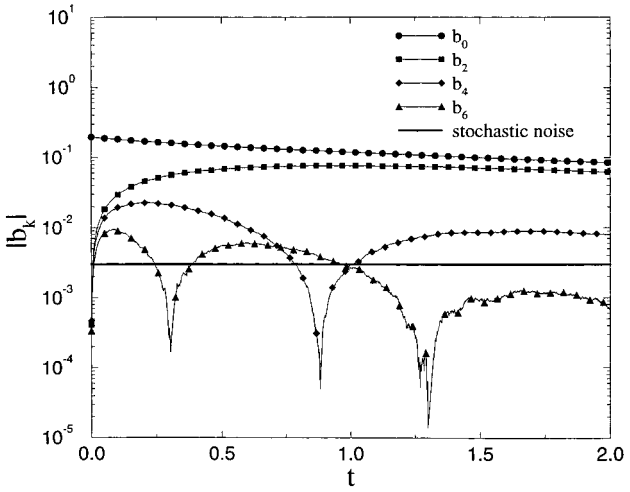

Figure 4. Amplitudes of the four largest Chebyshev coefficients b_k used to approximate the shear stress in the recovery of a dilute solution of FENE dumbbells at De = 49.62 and Re = 1.2757 compared to the stochastic noise in the shear stress.

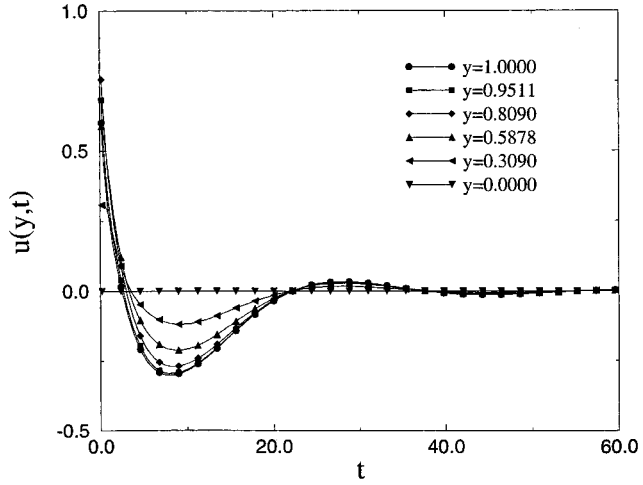

Figure 5. Time evolution of the velocities at the collocation points during the recovery of a dilute solution of FENE dumbbells at De = 49.62 and Re = 1.2757.

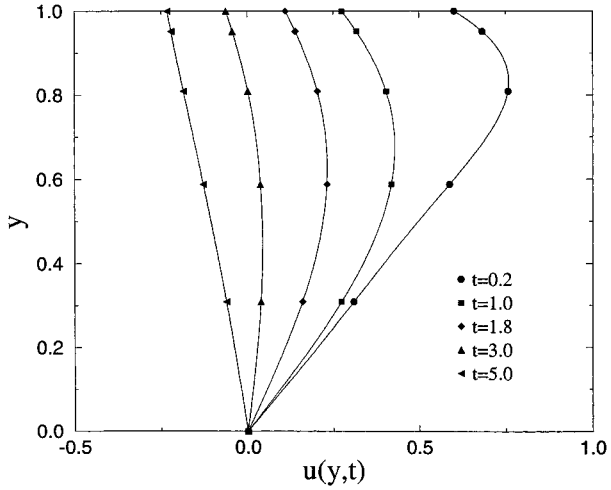

Figure 6. Velocity profiles $u(y,t)$ shortly after the start of recovery of a dilute solution of FENE dumbbells at De = 49.62 and Re = 1.2757.

are actually in the computational domain $y \in [0,1]$. A 10-point finite element method (FEM) using nodes at spatial positions identical to those of the 10-point spectral method, however, is shown to exhibit significant error. While a 20-point FEM solution leads to a decrease in this error, the result remains significantly less accurate than the 10-point spectral solution. An advantage of the spectral method is also illustrated in Figure 3 by the functions approximating the velocity between the collocation/FEM points. While the FEM interpolates between points using piecewise quadratic functions, the spectral method uses polynomials of the same order as the number of collocation points.

To quantify the effect of the number of collocation points on the calculated recovery, the stochastic fluctuations in the shear stress can be compared to the magnitude of the spectral coefficients b_k. These coefficients multiply the Chebyshev polynomials which are used to approximate τ_{yx}^{p} by eq 11. Figure 4 shows the absolute value of the four largest coefficients b_k during the simulation of Figure 3. The coefficients b_k are nonzero only for even k. The solid line in Figure 4 represents an upper bound on the stochastic noise in the shear stress, corresponding to a relative error of approximately 1%. Figure 4 shows that at longer times only three modes (b_0, b_2, and b_4) contribute to the stress; the contributions of higher modes are smaller than the stochastic noise. Even at very short times only four modes (b_0, b_2, b_4, and b_6) are observed to be significant, showing that a discretization of more than 10 collocation points does not influence the accuracy of the simulation.

Figure 5 shows the evolution of the velocity at each collocation point in the fluid for the same parameters as in the full spectral simulations represented by Figures 3 and 4. Figure 6 depicts the velocity profiles shortly after the beginning of the recovery simulation. At early times, the velocity profiles are highly nonlinear. In fact, the velocity gradient near the top plate at these early times is observed to be up to several times the imposed steady-state shear rate for higher values of $\lambda_H\dot{\gamma}$. This is significant, since Figure 5 shows that most of the overall recovery is due to the elastic response at short times. In the region very near the top plate much higher local shear rates occur than in the rest of the fluid, which experiences a nearly linear velocity profile and thus a shear rate close to that of the imposed steady-state value. Due to the shear thinning behavior of FENE dumbbells, the polymer contribution to the shear stress and therefore the magnitude of the elastic response is decreased preferentially in the region near the top plate. This additional shear thinning results in a smaller overall recovery and explains the difference between the two FENE dumbbell curves of Figure 2.

Figure 7 displays the steady-state viscosities of linear bead−spring FENE chains. Due to the scaling of nkT according to eq 16, the magnitudes of the stresses in the models are nearly independent of chain length. Most important is the fact that all FENE chain models exhibit significant shear thinning behavior over the range of shear rates investigated in this work. In light of this fact, it is not surprising that other FENE chain models have much the same overall recovery response as that displayed by the FENE dumbbell. Figure 8 summarizes the full spectral simulations for overall recovery of FENE chains. At high shear rates all models examined here exhibited a maximum in the overall recovery. The mechanism responsible for the maximum is again the ultimate dominance of inertial effects over increasingly insignificant elastic effects at high shear rates.

Results for simulations of the Curtiss−Bird melt model show behavior similar to that of the bead−spring

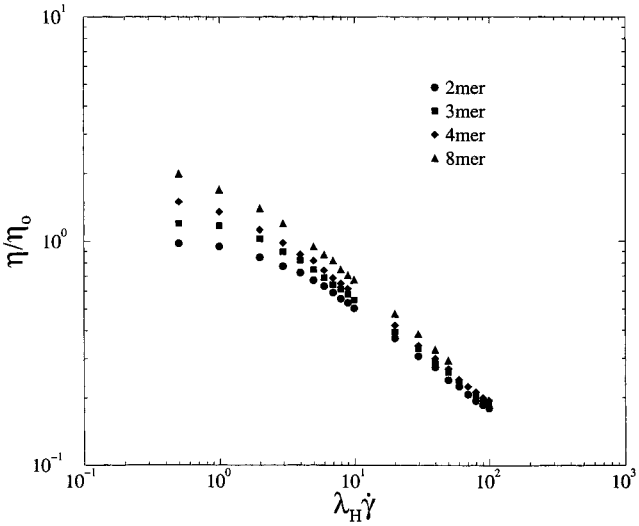

Figure 7. Steady-state shear viscosities of dilute solutions of bead−spring chains as a function of Deborah number $\lambda_H\dot{\gamma}$ and the FENE chain length.

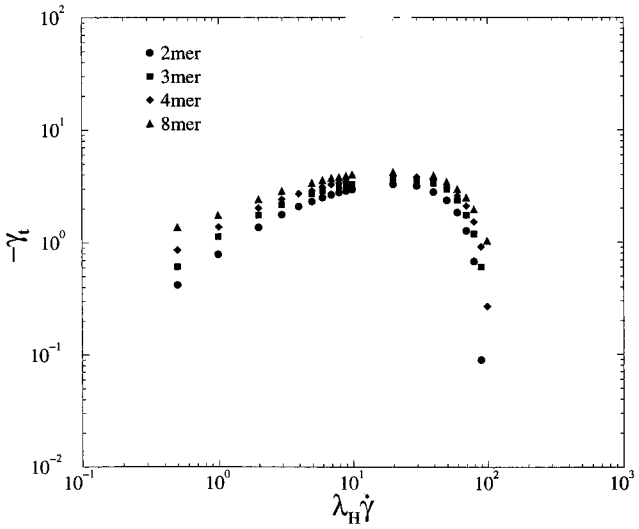

Figure 8. Overall recovery $-\gamma_t$ for bead−spring chains as a function of Deborah number $\lambda_H\dot{\gamma}$ and the FENE chain length.

chains in overall recovery. Figure 9 displays the viscosities computed in the steady shear flow before the start of the recovery simulation. The model exhibits significant shear thinning behavior over the relevant range of shear rates for all three values of link-tension coefficient. Figures 10 and 11 summarize simulations with the linear velocity profile assumption and the full spectral solution, respectively. A maximum in the overall recovery is again displayed at high shear rates. As in the FENE bead−spring chain simulations, the full spectral solution for the actual velocities causes much higher gradients near the top plate and leads to an even further decrease in the observed overall recovery. Figures 12 and 13 show highly nonlinear velocity profiles at early times decaying to linear velocity profiles at later times for the spectral simulation of a Curtiss−Bird melt model with De = $\lambda\dot{\gamma}$ = 400.0, Re = 0.141, and ϵ = 0.1.

The combined Brownian dynamics and spectral solution technique is moderately computationally demanding. The ensemble size at each collocation point was chosen on the basis of a criteria for acceptable noise in the steady-state shear stress signal. For bead−spring chains, this was approximately 10 000 trajectories per

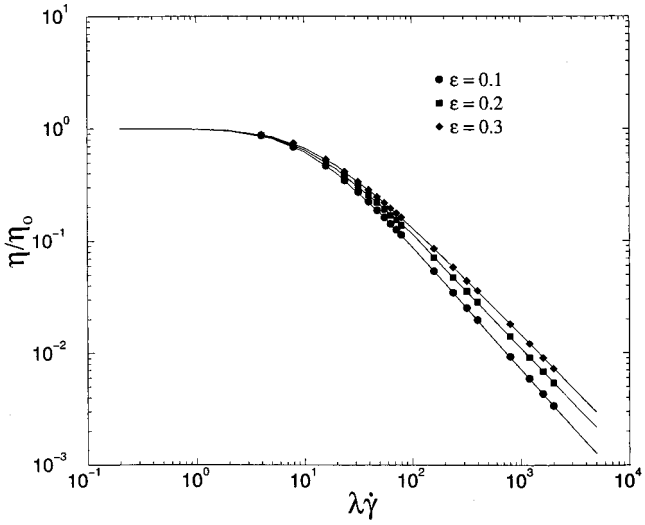

Figure 9. Steady-state shear viscosities of the Curtiss−Bird melt model as a function of Deborah number $\lambda\dot{\gamma}$ and the link-tension coefficient ϵ. Brownian dynamics simulation results are shown as points; results obtained from ref 5 are shown as solid lines.

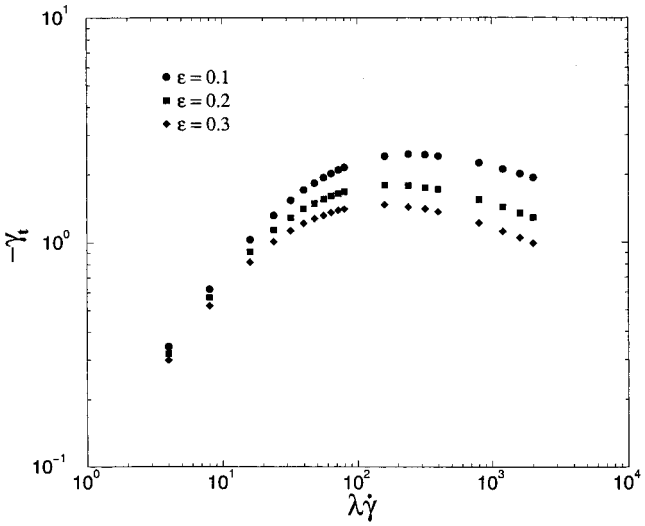

Figure 10. Ultimate recoil $-\gamma_\infty$ (assuming a linear velocity profile) for the Curtiss−Bird melt model as a function of Deborah number $\lambda\dot{\gamma}$ and the link-tension coefficient ϵ.

collocation point for dumbbells and 2000 trajectories for octamers. For the Curtiss−Bird simulations, 50 000 trajectories were sufficient. The time step used in the Brownian dynamics was chosen such that the correct steady-state shear viscosity would be obtained at the highest shear rate occurring in the recovery simulation; it ranged from 0.01 to 0.0001. At these time steps, numerical stability of the explicit Euler discretization of eq 10 was not an issue. A single simulation for overall recovery (one point on Figures 8, 10, or 11) required approximately 1 h of CPU time for dumbbells and Curtiss−Bird calculations at low shear rates to nearly 3 days of CPU time for FENE octamers at higher shear rates on a dedicated DEC alpha3000 workstation.

6. Conclusion

This brief paper describes the application of Brownian dynamics and spectral techniques to solution of macroscopic flow problems for polymeric liquids. The approach eliminates the need for a closed-form constitutive equation through the use of Brownian dynamics

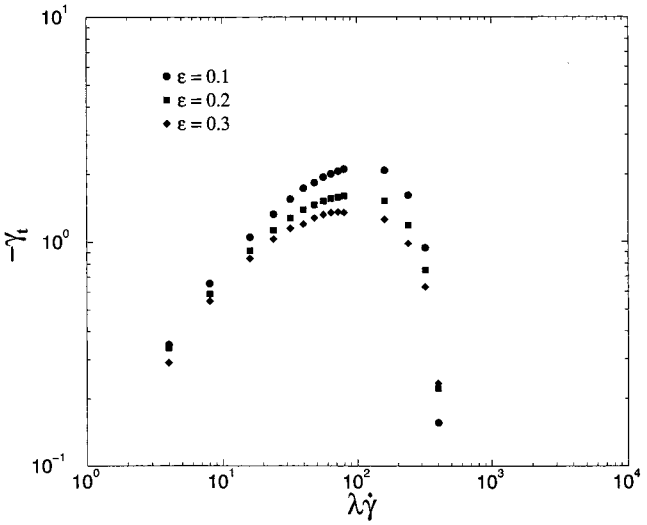

Figure 11. Overall recovery $-\gamma_t$ for the Curtiss−Bird melt model as a function of Deborah number $\lambda\dot{\gamma}$ and the link-tension coefficient ϵ. These calculations involve the simultaneous spectral and Brownian dynamics simulations for the shear stress and actual velocity profiles.

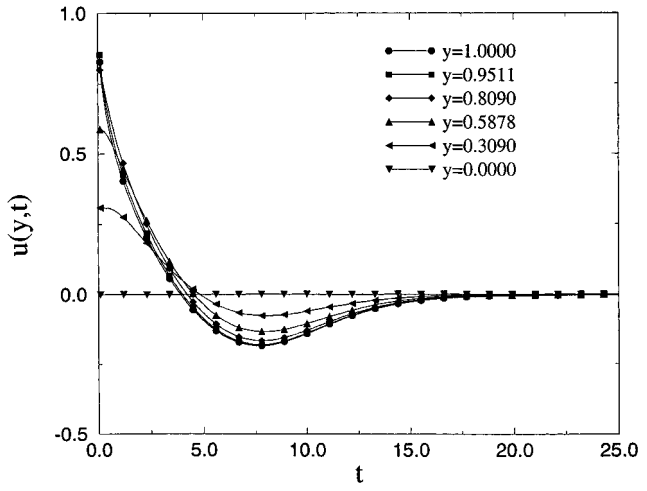

Figure 12. Time evolution of the velocities at the collocation points during recovery for the Curtiss−Bird model at De = 400.0 and Re = 0.141.

simulations and minimizes the number of such simulations that must be performed by exploiting a spectral discretization of the continuum equation of motion. A maximum in the overall recovery with increasing steady-state shear rate was found for both dilute solutions of FENE chains as well as the Curtiss−Bird model for melts. The shear thinning mechanism leading to this maximum was found to become even more important upon the removal of the assumption of linear velocity profiles throughout the fluid. The results presented here also demonstrate that the spectral technique is significantly more computationally efficient than the traditional finite element method in one dimension.

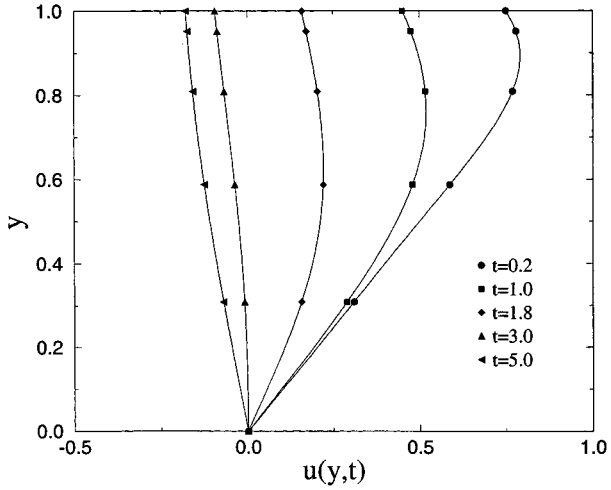

Figure 13. Velocity profiles $u(y,t)$ which occur shortly after the start of the recovery simulation for the Curtiss−Bird model at De = 400.0 and Re = 0.141.

Acknowledgment. G.H.N. thanks The Research Council of Norway for financial support from Grant No. 429.91/065. This work was partially supported by a Shell Faculty Fellowship, NSF CAREER Grant CTS-9502677, and ACS Grant ACS/PRF-28997-G9 to M.D.G. and by NSF NYI Grant CTS-9358406 and ACS Grant ACS/PRF-29399 to J.J.dP. The authors are grateful to H. C. Öttinger for helpful discussions and an anonymous reviewer whose insightful comments greatly improved the paper.

References and Notes

(1) Bird, R. B.; Armstrong, R. C.; Hassager, O. *Dynamics of Polymeric Liquids*; Wiley Interscience: New York, 1987; Vol. 1.
(2) Borgbjerg, U.; de Pablo, J. J.; Öttinger, H. C. *J. Chem. Phys.* **1994**, *101*, 7144.
(3) Bird, R. B.; Curtiss, C. F.; Armstrong, R. C.; Hassager, O. *Dynamics of Polymeric Liquids*; Wiley Interscience: New York, 1987; Vol. 2.
(4) Laso, M.; Öttinger, H. C. *J. Non-Newtonian Fluid Mech.* **1993**, *47*, 1.
(5) Öttinger, H. C. *Stochastic Processes in Polymeric Fluids*; Springer-Verlag: Berlin, 1996.
(6) Kloeden, P. E.; Platen, E. *Numerical Solution of Stochastic Differential Equations*; Springer-Verlag: Berlin, 1992.
(7) Gardiner, C. W. *Handbook of Stochastic Methods for Physics, Chemistry and the Natural Sciences*; Springer-Verlag: Berlin, 1985.
(8) Warner, H. R. *Ind. Eng. Chem. Fundam.* **1972**, *11*, 379.
(9) Gottlieb, D.; Orzag, S. A. *Numerical Analysis of Spectral Methods: Theory and Applications*; SIAM: Philadelphia, 1977.
(10) Cook, R. D.; Malkus, D. S.; Plesha, M. E. *Concepts and Applications of Finite Element Analysis*; Wiley: New York, 1989.
(11) Canuto, C.; Hussanini, M. Y.; Quarteroni, A.; Zang, T. A. *Spectral Methods in Fluid Dynamics*; Springer-Verlag: Berlin, 1988.
(12) Bell, T. W.; de Pablo, J. J.; Graham, M. D. Manuscript in preparation.

MA9602684